Preprint
UCRL-TR-201284

Evaporative Concentration of 100x J13 Ground Water at 60% Relative Humidity and 90°C

Q. A. Nguyen, P. Hailey, M. Sutton, K. Staggs, M. Alai, and S. Carroll

December 2003

U.S. Department of Energy

Lawrence
Livermore
National
Laboratory

This work was performed under the auspices of the U.S. Department of Energy by the University of California Lawrence Livermore National Laboratory under Contract No. W-7405-Eng-48.

Evaporative Concentration of 100x J13 Ground Water at 60% Relative Humidity and 90°C

Que Anh Nguyen, Phil Hailey, Mark Sutton, Kirk Staggs,
Maureen Alai, and Susan A. Carroll

Lawrence Livermore National Laboratory

December 4, 2003

Abstract

In these experiments we studied the behavior of a synthetic concentrated J13 solution as it comes in contact with a Ni-Cr-Mo-alloy selected for waste canisters in the designated high-level nuclear-waste repository at Yucca Mountain, Nevada. Concentrated synthetic J13 solution was allowed to drip slowly onto heated test specimens (90°C, 60% relative humidity) where the water moved down the surface of the specimens, evaporated and minerals precipitated. Mineral separation or zoning along the evaporation path was not observed. We infer from solid analyses and geochemcial modeling, that the most corrosive components (Ca, Mg, and F) are limited by mineral precipitation. Minerals identified by x-ray diffraction include thermonatrite, natrite, and trona, all sodium carbonate minerals, as well as kogarkoite (Na_3SO_4F), halite (NaCl), and niter (KNO_3). Calcite and a magnesium silicate precipitation are based on chemical analyses of the solids and geochemical modeling. The most significant finding of this study is that sulfate and fluoride concentrations are controlled by the solubility of kogarkoite. Kogarkoite thermodynamic data are needed in the Yucca Mountain Project database to predict the corrosiveness of carbonate brines and to establish the extent to which fluoride is removed from the brines as a solid.

---

1. Introduction

Yucca Mountain, located roughly 145 km NW of Las Vegas, Nevada, has been chosen as the first permanent geological repository for high-level nuclear waste. The designated repository will consist of 50 horizontal tunnels, about 1 km long and 5.5 m in diameter, where specially engineered waste containers will be stowed several hundred meters below the surface. Current designs call for a stainless steel (316L) container with a Ni-Cr-Mo alloy (Alloy 22) outer barrier, and a detached titanium alloy (grade 7) drip shield covering the waste packages. Alloy 22 and grade 7 Ti were chosen because they are highly resistant to corrosion (Yucca Mountain Science and Engineering Report 2001).

Electrochemical corrosion of the waste package outer barriers may occur when concentrated aqueous films form on the waste package surfaces, either by seepage water or moisture absorption by hygroscopic salts found in dust within the repository. Our research described in this report focuses on the composition and corrosiveness of evaporating seepage water. Seepage water is defined as evaporating pore water from the repository host rock that is transported to the drift tunnels where it can then drip onto the

waste package. Seepage water corrosiveness is dependent on the water composition, which is controlled by the precipitation of minerals as the water evaporates at elevated temperatures and diminished relative humidity over the lifespan of the repository. The chemical divide theory predicts that these dilute waters will evolve towards carbonate, sulfate, or calcium chloride brines (Li et al. 1997). Rosenberg et al. (2001) and Alai et al. (2003) have verified the evaporation of each of these water types on Yucca Mountain ground and pore water in batch experiments.

In these experiments we test the hypothesis that evaporation of dripping Yucca Mountain seepage water produces a distinct brine from those evaporated from a bulk solution (batch experiment) because the evaporating brine is physically separated from mineral precipitates. We monitor the geochemical evolution of dripping concentrated J13 water, a Na-carbonate Yucca Mountain ground water, as it evaporates on heated, inclined Alloy 22 specimens by identifying mineral and chemical composition at discrete locations on the Alloy 22 specimens. Solution compositions are also modeled using EQ3/6 geochemical code (Wolery and Jarek, 2003), and a high temperature Pitzer ion-interaction model (Pitzer 1991, Rard and Wijesinghe 2003) to complement the solid phase analyses.

2. Methods

2.1 Experimental Set-Up

To simulate water dripping onto the waste packages placed in the repository, a concentrated solution was dripped at the top of four heated specimens tilted at 20˚ in an environmental chamber held at 60% relative humidity and 90˚C. All specimens were factory mill finished Alloy 22, a Ni-Cr-Mo-alloy, of which two contained welds and two did not. One specimen did have crushed Topopah Spring tuff above its surface, in which the test solution traveled through the tuff before reaching the specimen to simulate ground water reacting with repository rock. The starting solution is a synthetic 100x J13 ground water (Table 1). It was prepared by dissolving the appropriate amount of reagent grade chemicals in de-ionized water to create 17 L of solution. The solution slowly dripped onto the specimens at a rate of 1 to 4 ml/hr, which permitted significant evaporation over the length of each specimen. Temperature was controlled and monitored with thermocouples attached to the upper right hand corner and bottom center of each specimen. Heaters were placed directly beneath the specimens. The experiment ran for about one month. Composition of the solution dripping off of the specimens was not analyzed because it continued to evaporate over the duration of the experiment. Solid run product mineralogy and chemical composition was determined by X-ray diffraction (XRD) and energy depressive spectroscopy (EDS) on powdered samples. Solids on each specimen were subdivided spatially to check for mineral and chemical separation as the brine evaporated on the inclined sample. The number of samples for a given specimen was determined by the presence of welds and mineral coverage and is indicated in Tables 2-5.

2.2. Solid Analyses

Mineralogy was determined by powdered XRD using a Cu-Kα source at 40 kV and 30 mA from 2 to 90° 2θ in 0.02° steps. The instrument was calibrated using NIST traceable silicon (# 640c) and mica (# 675) standards for high angle and low angle peaks,

receptively. XRD cannot detect amorphous solids or minerals that are present at < 2 wt%. Mineral identification was based the presence of a given mineral's three most intense peaks in the XRD pattern. In some cases where the most intense peaks overlapped with other mineral peaks, identification was based on the presence of lower intensity diagnostic peaks. A mineral is listed as possibly present if all of its peaks overlap with other mineral peaks.

Semi-quantitative elemental analyses were conducted by EDS using an FEI Quanta 200 environmental scanning electron microscope. Powder samples were scanned at 20 kV at low magnification (100x) and are representative of the bulk composition. Energy spectrum calibration was verified using a NIST-traceable standard (# C2402).

2.3. Modeling Evaporation

Solution compositions were modeled using EQ3/6 geochemical code (Wolery and Jarek 2003), and a high temperature Pitzer ion-interaction model (Pitzer 1991, Rard and Wijesinghe 2003). The high temperature Pitzer ion-interaction model approximates non-ideal behavior of solutions at elevated ionic strength and temperatures. The evaporation model simulated the drip process in our experiments and was run sequentially from the initial concentration of 100x to 1000x, 1,000x to 10,000x, and 10,000 to 100,000x in which the concentrating brine was separated from the solids at each 10x interval. Mineral precipitation was suppressed for quartz and dolomite because of slow kinetics; for glaserite and magnesite because the available thermodynamic data are questionable; and for talc because it is not expected to form in a rhyolitic repository. Calculated solution results are electrically balanced by adjusting sodium concentration with a convergence tolerance of 0.1ppb. The output pickup file generated in the first EQ3 run, which calculates the 90˚C starting composition from the 25˚C experimental starting solution, was then incorporated into the input file for evaporation models using EQ6v8.0 reaction path code. Pressure varied according to the 1.013-bar/steam-saturation curve, and the oxygen and carbon dioxide fugacity were fixed at 20% and 0.01% respectively.

3. Results

3.1 XRD Data

Tables 2-5 show the spatial distribution of the minerals found on the Alloy 22 specimens (DTN: LL030805812251.068). In general, similar mineral assemblages are detected from top to bottom of the Alloy 22 specimens, indicating minimal physical separation of the solution from the precipitates along the evaporation path. The most common and dominant minerals identified are kogarkoite (Na_3FSO_4), halite (NaCl) and thermonatrite ($Na_2CO_3 \cdot H_2O$). Other minerals found in the samples are natrite (Na_2CO_3), and trona ($Na_3H(CO_3)_2 \cdot H_2O$). Although trona precipitated only on the specimens without welds it is doubtful that the weld had any direct impact on the mineral formed, because sodium carbonates precipitated on all four specimens. Furthermore, it is doubtful that precipitation of trona is due to reactions of the solution with tuff, because trona was identified on specimens with and without tuff. Precipitation of niter (KNO_3) could not be uniquely identified, because its major peaks overlap with the peaks of the more abundant salts. There were no detectable amounts of sylvite (KCl), calcite ($CaCO_3$) or magnesium silicate minerals.

3.2 Energy Depressive Analysis

In Figure 1, we average carbon, fluorine, sulfur, chlorine, and potassium concentrations across each specimen and show the chemical composition of the mineral precipitates from top to bottom of each specimen, because we observed no distinct trends in the data and because the evaporation path is variable over the course of the experiment. Any nitrogen present in the samples is included in the oxygen value, because nitrogen is partially masked by oxygen. It is important to remember, that the EDS analyses reported here are semi quantitative in nature (thus not qualified by the Yucca Mountain Project), and only provide a rough indication of chemical abundance. We use the EDS data to indicate relative mineral abundance by correlating carbon to sodium carbonate phases (natrite, thermonatrite, and trona), fluorine and sulfur to kogarkoite, chlorine to halite and potassium to niter. Sodium carbonate minerals are the most abundant phases, followed by kogarkoite, halite and niter. Measurement of trace amounts of magnesium and silica are consistent with the precipitation magnesium silicates and amorphous silica (or another SiO_2 polymorph). The final amount of magnesium and silica in the solids is small and below the detection of XRD. No calcium is detected by EDS, indicating that at most trace amounts precipitated.

3.3 *Modeling*

Figures 2 and 3 show the calculated evolution of mineral and solution composition for simulation 100x J-13 water as it drips down the specimen and evaporates (DTN: LL030805812251.068). Model calculations predict the precipitation of calcite, sepiolite ($Mg_4Si_6O_{15}(OH)_2 \cdot 6H_2O$), fluorite ($CaF_2$), villiaumite (NaF), thenardite (Na_2SO_4), natrite, halite, and cristobalite (SiO_2). Generally, the model agrees with experiment and predicts sodium carbonate, fluorides, sulfates, and halite to be the most abundant phases and trace amounts of cristobalite, calcite and magnesium silicates. The primary difference between the prediction and the experimental results is that fluoride and sulfate precipitate as kogarkoite and not as distinct fluorite, villiaumite, and thenardite phases. Kogarkoite solubility data is not available in the Yucca Mountain Project thermodynamic data base. The model does predict separation of calcite in the early stages of evaporation that was not seen in our experiments. If calcite and magnesium silicates precipitated in our experiments, the amounts are too small to detect. The model predicts an alkaline (pH > 10) Na-K-NO_3-Cl-CO_3-SO_4 brine with significant F (about $10^{-0.5}$ molal) and trace concentrations of Ca and Mg (less than 10^{-5} molal).

4. Discussions

4.1 Important Chemical Divides

The chemical divide theory describes the chemical evolution of dilute waters upon evaporation in terms of their equivalent calcium, sulfate and bicarbonate ratios (Hardie and Eugster 1970, Li et al., 1997). The chemical evolution of evaporating waters is controlled by the high solubility of salt minerals relative to the moderate solubility of calcium sulfate and low solubility of calcium carbonate minerals. An alkaline pH, carbonate brine (Na-K-**CO_3**-Cl-SO_4-NO_3) forms from dilute waters with dissolved calcium that is less than the dissolved carbonate (Ca < HCO_3+CO_3, equivalent %). A

near neutral pH, sulfate brine (Na-K-Mg-Cl-**SO_4**-NO_3) forms from dilute waters with dissolved calcium that is greater than the dissolved carbonate, but less than the combined dissolved sulfate and carbonate ($Ca < SO_4+HCO_3$, equivalent %). A Ca-chloride brine with near neutral pH (Na-K-**Ca**-Mg-Cl-NO_3) forms from dilute waters with dissolved calcium that is greater than the combined dissolved sulfate and carbonate ($Ca > SO_4+HCO_3$, equivalent %).

Dilute and concentrated synthetic J13 waters are classified as carbonate waters because they contain more carbonate alkalinity than dissolved calcium. In addition to the calcium chemical divides described above, drip (this study) and batch (Rosenberg et al., 2001) experiments confirm the importance of amorphous silica, magnesium silicate, and sodium carbonate chemical divides in controlling carbonate brine composition. The primary difference between chemical divides identified for the evaporation of J13 water in our drip experiment and Rosenberg et al (2001) batch experiment is that kogarkoite precipitation controls the solubility of sulfate and fluoride. Rosenberg et al (2001) did not identify a solubility controlling phase for fluoride (although hectorite ($Na_{0.33}Mg_3Si_4O_{10}(F,OH)_2$ may be present). Kogarkoite is a rare mineral, but it has been detected in thermal spring sediments in Colorado (Sharp 1970, Pabst and Sharp 1973). The sediments contain opal (amorphous silica), burkeite ($Na_6(CO_3)(SO_4)_2$), trona, halite, fluorite, and calcite and evolve from a dilute spring water with minimal calcium (8.5×10^{-5} M) compared to fluoride (6.8×10^{-4} M), carbonate ($HCO_3^- = 7.2 \times 10^{-4}$M, $CO_3^{2-} = 3.2 \times 10^{-4}$ M) and sulfate (1.1×10^{-3} M). This spring water is dominated by sulfate and is distinct from the synthetic sodium carbonate water used in the drip experiment. The current Yucca Mountain Project database uses the solubility of villiaumite (NaF) to limit fluoride concentrations and yields brines with about 0.15 molal F-. It is possible that kogarkoite has a lower solubility than villiaumite, because it is a mixed salt containing the less soluble thenardite (Na_2SO_4) component. Thermodynamic data are available to only 30°C for kogarkoite (Gurevich et al 1999), which is far below the range needed to describe environments in the repository.

4.2 Impact of carbonate brines on Alloy 22 corrosion.

Current waste package design for the disposal of high-level radioactive waste in the designated repository in Yucca Mountain, Nevada, USA calls for a Ni-Cr-Mo alloy as the outer barrier of the waste canisters and a titanium drip shield, because these materials are highly resistant in most solutions. Solutions that tend to induce corrosion on these materials have high calcium chloride, magnesium chloride concentrations and fluoride concentrations (Yucca Mountain Science and Engineering Report 2001). The J13 ground water and over half of the pore water sampled from the Topopah Spring Tuff repository formation (Alai et al., 2003) are classified as carbonate waters. Studies indicate that Alloy 22 corrosion is slightly enhanced in carbonate brines. Alloy 22 corrosion rates measured from five year experiments at 90°C in nominal 1000x J13 water are at most 10 times greater than Alloy 22 corrosion in dilute J13 waters (Wong et al. 2004). In the same 5 year experiments, corrosion rates for grade 7 titanium are about 40±8 nm/yr in 1000x J13 water and nondectable in dilute J13 water (Wong et al. 2003). It seems likely that higher fluoride concentrations in brines is responsible for the slightly higher corrosion rates. The 1000x J13 waters contained about 1400 ppm F- (about 0.07 M) and no detectable Ca or Mg. The fluoride concentration of the 1000x J13 waters are 100

times higher than the dilute J13 waters. Fluoride concentrations may be only partially limited by mineral solubility as sodium carbonate waters evaporate. Fluoride concentrates to about 700 times (about 0.08 M) its initial value after 99.9% evaporation in batch experiments (Rosenberg et al. 2001). In our drip evaporation experiments, fluoride solubility is controlled by the precipitation of kogarkoite. As discussed above, precipitation of kogarkoite may further lower fluoride concentration in the brine, making these brines less corrosive than those formed in the batch experiments.

Brines evolving from the evaporation of carbonate brines should be low in calcium and magnesium, because these elements are removed from solution by the precipitation of calcite and magnesium silicate, as is predicted by the geochemcial calculations of this drip experiment. Calcite, aragonite ($CaCO_3$), smectite ($Na_{0.3}(Al,Mg)Si_4O_{10}(OH)_2$) and possibly hectorite ($Na_{0.33}Mg_3Si_4O_{10}(F,OH)_2$) were identified in a batch evaporation experiment of dilute J13 water, which limited Ca and Mg concentrations to less than 5 times their initial values after 99.9 percent evaporation (Rosenberg et al. 2001). The reason no carbonates or magnesium silicates were detected in the drip evaporation experiments is that small amounts of bicarbonate, calcium, magnesium, and silica were used in the initial 100x J13 water to mimic carbonate and magnesium silicate precipitation in the initial states of evaporation from 1x to 100x. These relatively low concentrations of calcium, magnesium, and silica are predicted to yield less than 1% of each calcite and sepiolite, and would not be detectable by XRD. The initial 100x J13 drip water contained about 100 times the sodium, potassium, chloride, nitrate and fluoride concentrations; 50 times bicarbonate concentrations; and less than 10 times calcium, magnesium, and silica concentrations than the dilute J13 water used in the batch experiment.

5. Conclusions

Minerals formed from a 100x synthetic J13 ground water as it dripped down Alloy 22 alloy specimens and evaporated at 90˚C and 60% relative humidity included natrite, trona, thermonatrite, kogarkoite, halite, niter, and possibly calcite and magnesium silicates. Prediction of brine composition and corrosiveness formed from seepage water and the deliquescence of salts precipitated from the seepage waters should include kogarkoite solubility, because kogarkoite was identified as the solubility controlling phase for fluoride and sulfate in carbonate type waters that are similar to measured Yucca Mountain pore waters.

REFERENCES

Alai, M. and Carroll, S. (2003) Evaporative evolution of brines from synthetic Topopah Spring Tuff pore water, Yucca Mountain, NV. Materials Research Society Symposium Proceedings, **757**, 579-585.

DTN: LL030805812251.068 (2003) Corrosion testing on heat transfer surfaces; electrolyte drip testing.

Hardie, L.A. and Eugster, H.P. (1970) The evolution of closed-basin brines. *Mineral. Soc. Amer. Spec. Pap.* **3**, 273-290.

Li, J., Lowenstein, T. K., and Blackburn, I. R. (1997) Responses of evaporite mineralogy to inflow water sources and climate during the past 100 k.y. in Death Valley, California. *GSA Bulletin*, **109**, 1361-1371.

Gurevich, V. M., Gorbunov, V. E., Gavrichev, K. S., and Khodakovskii, I. L. (1999) A calorimeter for heat capacity measurements from 50 to 300 K: The heat capacities of kogarkoite Na_3SO_4F(cr) at low temperatures. *Geochemistry International*, **37**, 367-377.

Pabst, A. and Sharp, W. N. (1973) A new natural phase in the system Na_2SO_4-NaF-NaCl, *Am. Mineral.*, **58**, 116-127.

Pitzer, K. S. (1991) Ion Interaction Approach: Theory and Data Correlation. In *Activity Coefficients in Electrolyte Solutions*, 2nd. ed.; K. S. Pitzer, Ed.; CRC Press: Boca Raton, FL, 75–153.

Rard, J. A. and Wijesinghe, A. M. (2003) Conversion of parameters between different variants of Pitzer's ion-interaction model, both with and without ionic strength dependent higher-order terms. *J. Chemical Thermodynamics*, **35**, 439–473.

Rosenberg, N. D., Gdowski, G. E., and Knauss, K. G. (2001) Evaporative chemical evolution of natural waters at Yucca Mountain, Nevada. *Applied Geochemistry*, **16**, 1231-1240.

Sharp, W. N. (1970) Extensive zeolitization associated with hot springs in central Colorado. U.S. Geol. Surv. Prof. Pap., **700-B**, B14-B20.

Wolery, T. J. and Jarek, R. L. (2003) *EQ3/6, Version 8.0, Software User's Manual*, Software U.S. Department of Energy, Office of Civilian Radioactive Waste Management, Document Number: 10813-UM-8.0-00, Las Vegas, NV.

Wong, L. L., Estil, J. C. Fix, D. V., Rebak, R. B. (2003) Corrosion characteristics of titanium alloys in multi-ionic environments. Transportation, Storage, and Disposal of Radioactive Materials, **PVP-467**, 63-71.

Wong, L. L., Lian, T., Fix, D. V., Sutton, M., and Rebak, R. B. (2004) Surface analysis of Alloy 22 samples exposed for five years to concentrated ground waters. *Corrosion/04* (in press).

Yucca Mountain Science and Engineering Report (2001) U. S. Department of Energy, Office of Civilian Radioactive Waste Management, DOE/RW-0539, Las Vegas, NV.

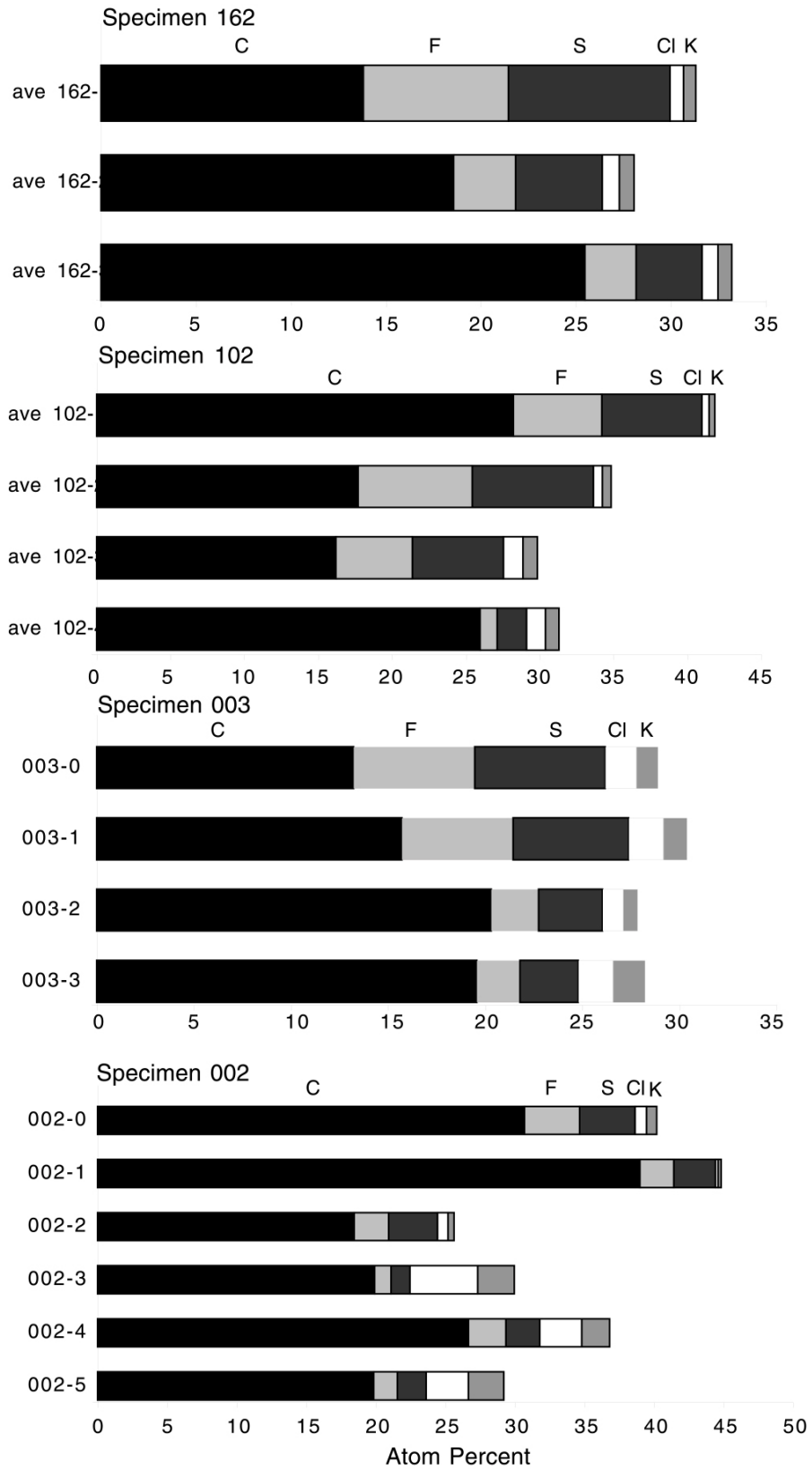

Figure 1. The average C, F, S, Cl, and K atom percent composition of the mineral precipitates from top to bottom of each Alloy 22 specimen.

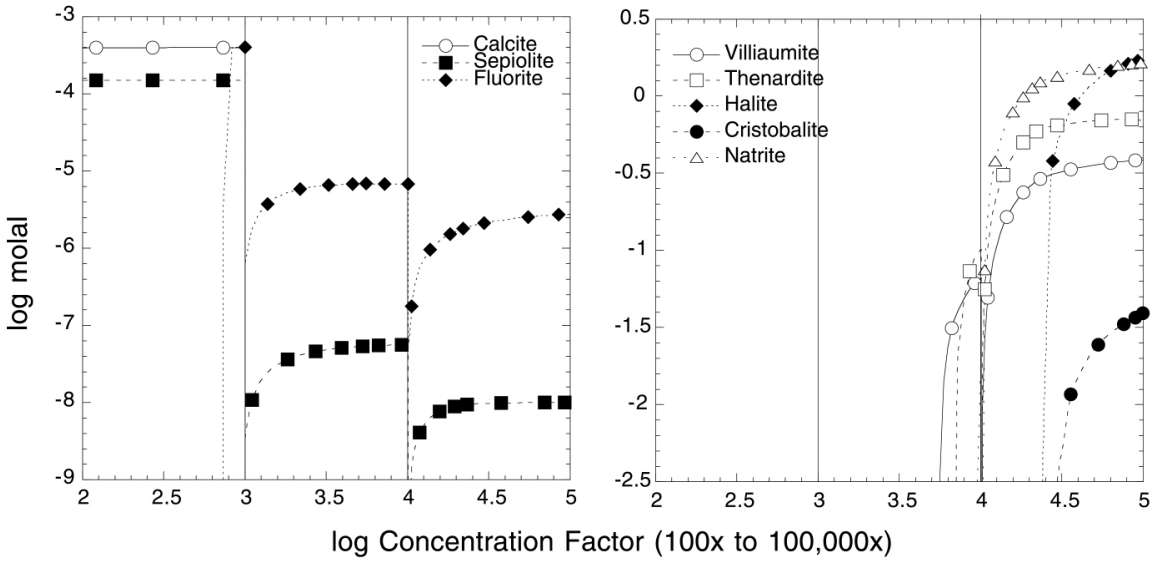

Figure 2. Predicted mineral precipitation upon evaporation of the starting 100x J13 water. Solution composition is separated from solids at each 10x concentration factor in an effort to mimic the drip experiments.

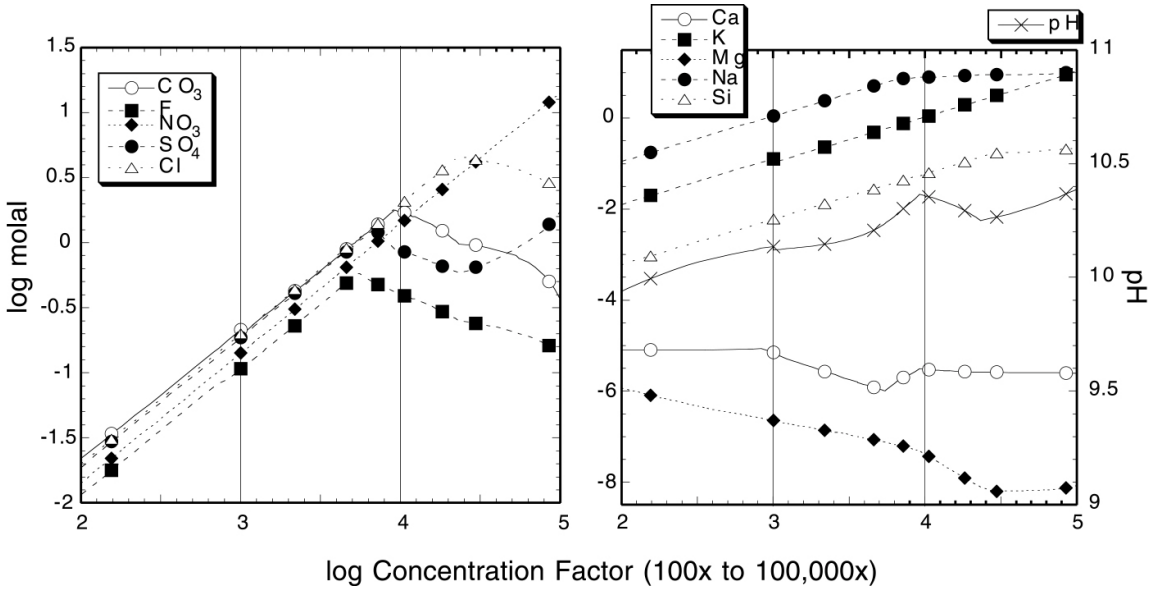

Figure 3. Predicted water chemistry upon evaporation of the starting 100x J13 water. Solution composition is separated from solids at each 10x concentration factor in an effort to mimic the drip experiments.

Table 1. Composition of concentrated J13 water used in drip experiments.

Element	Molal (mol/Kg solvent)
Na	0.1856
HCO_3	0.0814
Cl	0.0198
SO_4	0.0187
NO_3	0.0141
K	0.0127
F	0.0114
Si	0.0015
Mg	0.0006
Ca	0.0004

Table 2. Minerals identified on Specimen 162 with a weld down the center of column B.

A	B
162-1a.	
Kogarkoite	
Halite (possibly present)	
162-2a	**162-2b**
Kogarkoite	Kogarkoite
Halite	Natrite
Natrite	Halite
Niter (possibly present)	Niter (possibly present)
162-3a	**162-3b**
Natrite	Natrite
Thermonatrite	Thermonatrite
Halite	Halite
Kogarkoite	Kogarkoite
Niter (possibly present)	Niter (possibly present)

Table 3. Minerals identified on Specimen 102 *with* welds run down the center of column B and C.

A	B	C
	102-1ABC Kogarkoite Natrite Halite (possibly present) Thermonatrite (possibly present)	
102-2a Kogarkoite Halite Thermonatrite (possible)	**102-2b** Kogarkoite Halite Thermonatrite (possible)	**102-2c** Kogarkoite Halite Thermonatrite (possible)
102-3a Kogarkoite Halite Thermonatrite Natrite (possible)	**102-3b** Kogarkoite Halite Thermonatrite	**102-3c** Kogarkoite Halite Thermonatrite Natrite (possible)
102-4a Natrite Thermonatrite Halite Kogarkoite (possible) Niter (possible)	**File: 102-4b** Thermonatrite Natrite Halite Kogarkoite Niter (possible)	**102-4C** Thermonatrite Halite Kogarkoite Natrite (possible)

Table 4
Minerals identified on Specimen 003 with tuff deposits, no welds

003-0
Kogarkoite
Trona
Halite
Thermonatrite (possible)
Niter (possible)
003-1
Kogarkoite
Trona
Halite
Niter
Thermonatrite (possible)
003-2
Thermonatrite
Halite
Trona
Kogarkoite
Natrite (possible)
003-3
Thermonatrite
Halite
Kogarkoite
Niter

Table 5. Minerals identified on Specimen 002 without tuff, no welds.

002-0
Kogarkoite
Trona
Halite
Thermonatrite
Niter (possible)
002-1
Thermonatrite
Kogarkoite
Trona
Halite
002-2
Thermonatrite
Kogarkoite
Trona
Halite
Natrite (possible)
002-3
Halite
Kogarkoite
Thermonatrite
Niter
002-4
Halite
Kogarkoite
Thermonatrite
Niter
Trona (possible)
Natrite (possible)
002-5
Halite
Kogarkoite
Thermonatrite
Niter (possible)
Natrite (possible)